Materials and Structures, 1992, **25**, 21–28

Improved prediction model for time-dependent deformations of concrete: Part 3–Creep at drying

ZDENĚK P. BAŽANT, JOONG-KOO KIM

Center for Advanced Cement-Based Materials, Northwestern University, Evanston, Illinois 60208, USA

Part 3 of the present series gives the prediction formulae for the average compliance function in the cross-section of a specimen exposed to drying at constant temperature. The formulae describe the additional creep due to drying by means of the shrinkage function, which automatically introduces the consequences of diffusion theory, such as the dependence of creep on cross-section thickness and shape. The prediction formulae are compared with 19 different data sets from the literature, which reveal relatively good agreement, better than that with previous models. The main source of error is insufficient knowledge of the effect of mix composition and concrete strength. It is advisable to avoid this error by carrying out short-time measurements whenever possible.

1. INTRODUCTION

When a concrete specimen that creeps under load is simultaneously exposed to a drying environment, its deformation is much larger than the sum of the shrinkage of a load-free specimen and the creep with elastic deformation of a loaded sealed specimen. This phenomenon, known as the Pickett effect [1], can be regarded as either additional stress-induced shrinkage or as additional drying creep. Both viewpoints are mathematically equivalent [2]. We chose the latter viewpoint, namely that of additional drying creep, as in the original BP model [3].

2. FORMULAE FOR CREEP AT DRYING

The average compliance function for a cross-section of a long member, representing the sum of the instantaneous deformation, the basic creep and the additional creep due to drying, can be expressed as

$$J(t,t',\sigma)=q_1+F(\sigma)[C_0(t,t')+C_d(t,t',t_0)+C_p(t,t',t_0)] \quad (1)$$

in which q_1 represents the instantaneous deformation, the same as for basic creep; $C_0(t,t')$ represents the basic creep (Part 2 [4]); $C_d(t,t',t_0)$ represents the additional creep due to simultaneous drying; and $C_p(t,t',t_0)$ represents a further creep increase due to predrying, which can be neglected in most cases, except when the time lag $(t'-t_0)$ is large and the member is thin; t' = age at loading, t_0 = age at the start of drying and t = current age (all in days).

As shown in Appendix II of Bažant and Chern [2], integration of the differential equation for the additional creep rate caused by the time rate of pore relative humidity indicates, under certain simplifying assumptions, that the drying creep term should approximately be a function of the increase of the average shrinkage strain during the period of loading. Based on this argument, the creep during drying is expressed approximately as

$$C_d(t,t',t_0)=q_5k_h'\varepsilon_{sh,\infty}\left[S\left(\frac{t-t_0}{\tau_m}\right)-S\left(\frac{t'-t_0}{\tau_m}\right)\right]^{1/2} \quad (2)$$

in which S is a function already defined for shrinkage (Equation 2 in Part 1 [5]); q_5 = empirical constant; $\varepsilon_{sh,\infty}$ = final shrinkage strain for zero humidity, given by Equation 7 in Part 1 [5]; and the halftime τ_m is similar but not exactly the same as the shrinkage halftime τ_{sh}. It is expressed as

$$\tau_m=2\left(1+\frac{3.5}{t_0^{1/2}}\right)\left(1+\frac{5}{(t'+t_0)^{1/2}}\right)^{-1}\tau_{sh} \quad (3)$$

(all times in days). The first and second correction terms are empirical, although the first one is approximately proportional to the inverse of diffusivity $C_1(t_0)$ for shrinkage (Equation 6 of Part 1 [5]).

The additional creep due to predrying from t_0 to t' is related to the magnitude of shrinkage from t_0 to t' and is given by the semiempirical expression

$$C_p(t,t',t_0)=0.7k_h''\left[\frac{1}{G(7+t_0)}-0.9^{1/2}\right]\left[S\left(\frac{t'-t_0}{0.5\tau_m}\right)-S\left(\frac{t'-t_0}{5\tau_m}\right)\right]C_0(t,t') \quad (4)$$

where function G is defined in Equation 15, Part 1 [5]. The appearance of τ_{sh} in Equation 3 automatically introduces the main consequences of diffusion theory, particularly the dependence of drying creep and predrying creep on the cross-section thickness and shape, diffusivity at the start of drying and temperature as given by Equations

0025-5432/92

3–10 of Part 1 [5] for shrinkage. The humidity dependence is similar to but slightly different from that in Part 1:

$$k'_h = h_0^3 - h^3 \qquad k''_h = h_0^2 - h^2 \tag{5}$$

in which h = relative environmental humidity, assumed to be constant, and h_0 = initial pore relative humidity at which the specimen was in moisture equilibrium before time t_0 (usually $h_0 = 0.98$ to 1.00). The empirical constant 0.7 ensues from the data in Simenov and Bozhinov [6].

The additional creep due to predrying may be explained by the fact that predrying causes the degree of hydration to be less than in specimens exposed simultaneously with loading, and a lower degree of hydration means a higher creep. It must be pointed out, however, that the present expression for C_p does not apply for very long predrying times such as $t' - t_0 \gg \tau_{sh}$, in which case a new moisture equilibrium state is closely approached already before loading. In that case, i.e. for dried specimens that have already reached equilibrium (which can only be achieved with very thin specimens), the lower the environmental humidity the smaller is creep; then functions C_d and C_p need to be dropped and $C_0(t, t')$ needs to be multiplied approximately by the term $(0.1 + 0.9h_0^2)$.

Equations 2–5 represent various well-established properties of drying creep:

(a) Drying that proceeds simultaneously with creep intensifies creep (while the loss of water that occurred previously reduces creep if moisture equilibrium in the pores has already been attained).

(b) The increase of creep due to drying depends on the environmental humidity and the size and shape of the cross-section similarly to shrinkage, as reflected in k'_h and τ_{sh}. For very thick specimens ($\tau_{sh} \to \infty$) the drying effect on the average creep in the cross-section disappears.

(c) Similar to shrinkage, the increase of creep due to drying is higher at a lower age.

(d) The later the concrete is loaded after the start of drying, the smaller is the increase of creep due to drying (which is more pronounced for a thinner specimen).

(e) The creep increase due to drying is delayed compared to shrinkage, which is approximately described by introducing the exponent 1/2 into Equation 2. The first parenthetic expression in Equation 4 reflects the fact that the strength decrease due to drying before loading increases creep (this term vanishes when $t_0 \to \infty$, i.e. for the end of hydration).

One important difference between basic creep and additional creep due to drying is that the former does not have any asymptotic final value while the latter does. Also the slope of the curve of creep versus the logarithm of load duration never decreases for the basic creep, but it does decrease for the drying creep.

Effects of humidity cycling can be added to the present prediction equations in the form proposed by Bažant and Wang [7]. They are negligible for thicker specimens because the environmental humidity fluctuations penetrate only to a small depth in concrete (see also Part 5).

3. PREDICTION OF MATERIAL PARAMETERS FROM COMPOSITION AND STRENGTH

By analysis of numerous test data it was verified that

$$q_5 = \frac{40}{(f'_c)^{1/2}} \tag{6}$$

in which f'_c = 28-day cylinder strength in psi (1 psi = 6895 Pa). The formula for predicting ε_{sh_∞} has already been given in Part 1 [5].

The effects of carbonation, as well as admixtures, pozzolans, fly-ash and silica fume, are not included in the present parameter prediction (however, adjustment by parameters $\alpha_1, \ldots$ explained later can handle them). Since carbonation usually penetrates only a very thin layer of concrete (2 to 10 mm), it must have a negligible effect on concrete members of normal thickness.

4. PREDICTION IMPROVEMENT BASED ON SHORT-TIME DATA

Since prediction of material parameters from composition and strength is the main source of error, one can greatly improve the predictions by adjusting the parameters according to short-time creep data. Similar to the procedure described in Part 2 [4] (Equation 13), first the parameters $q_1, \ldots, q_5$ are predicted from the present formulae and then they are replaced by

$$\alpha_1 q_1, \alpha_1 q_2, \alpha_1 q_3, \alpha_1 q_4, \alpha_1 q_5 \tag{7}$$

Unknown coefficient α_1 is then determined (e.g. by trial and error) to get the best fit of the available data for the concrete to be used.

If more extensive data covering a longer creep period are available, $q_1, \ldots, q_5$ are predicted from the present formulae and are then replaced by

$$\alpha_1 q_1, \alpha_2 q_2, \alpha_2 q_3, \alpha_2 q_4, \alpha_2 q_5 \tag{8}$$

Unknown coefficients α_1 and α_2 are then determined (by linear regression) to get the best fit of the existing data.

If the data include not only longer times but also creep with or without drying, $q_1, \ldots, q_5$ are predicted from the present formulae and are then replaced by

$$\alpha_1 q_1, \alpha_2 q_2, \alpha_2 q_3, \alpha_2 q_4, \alpha_3 q_5 \tag{9}$$

Unknown coefficients α_1, α_2 and α_3 are then determined by linear regression of the available data.

All the parameters $q_1, \ldots, q_5$ cannot be determined unless the data cover the whole range, including small and high ages at loading.

In this manner the present prediction formulae are used to determine only the ratios between the parameters $q_1, \ldots, q_5$, not their magnitudes. As far as these ratios are concerned, the errors of the present formulae are much less than in terms of the magnitudes. As the data base increases it is further possible to determine from the present prediction formulae only some ratios of $q_1, \ldots, q_5$ and obtain the other ratios (e.g. q_1/q_2) directly from test data, which further eliminates part of the error.

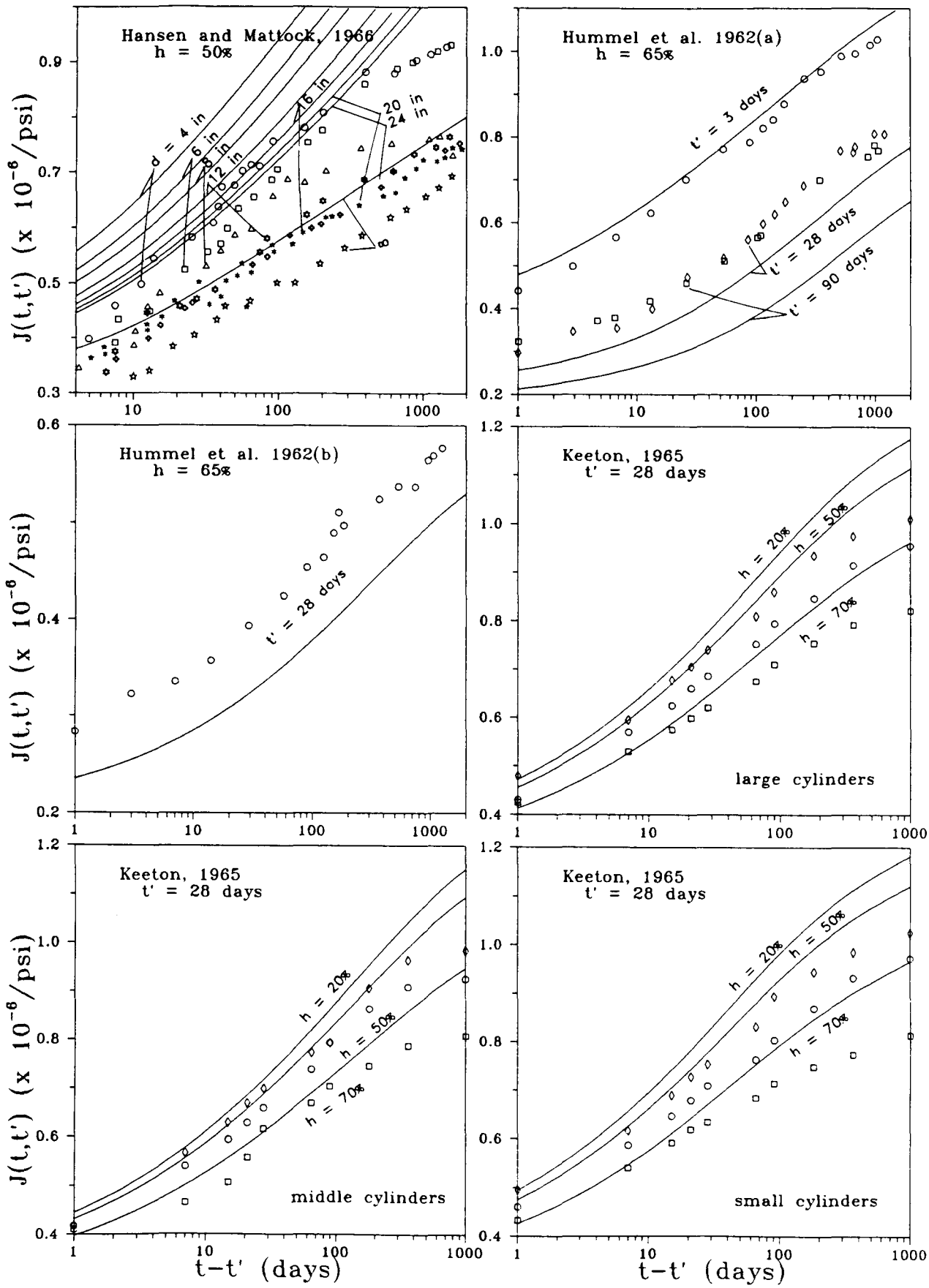

Fig. 1 Predictions of drying creep and data by Hansen and Mattock [8], Hummel *et al.* [9] and Keeton [10].

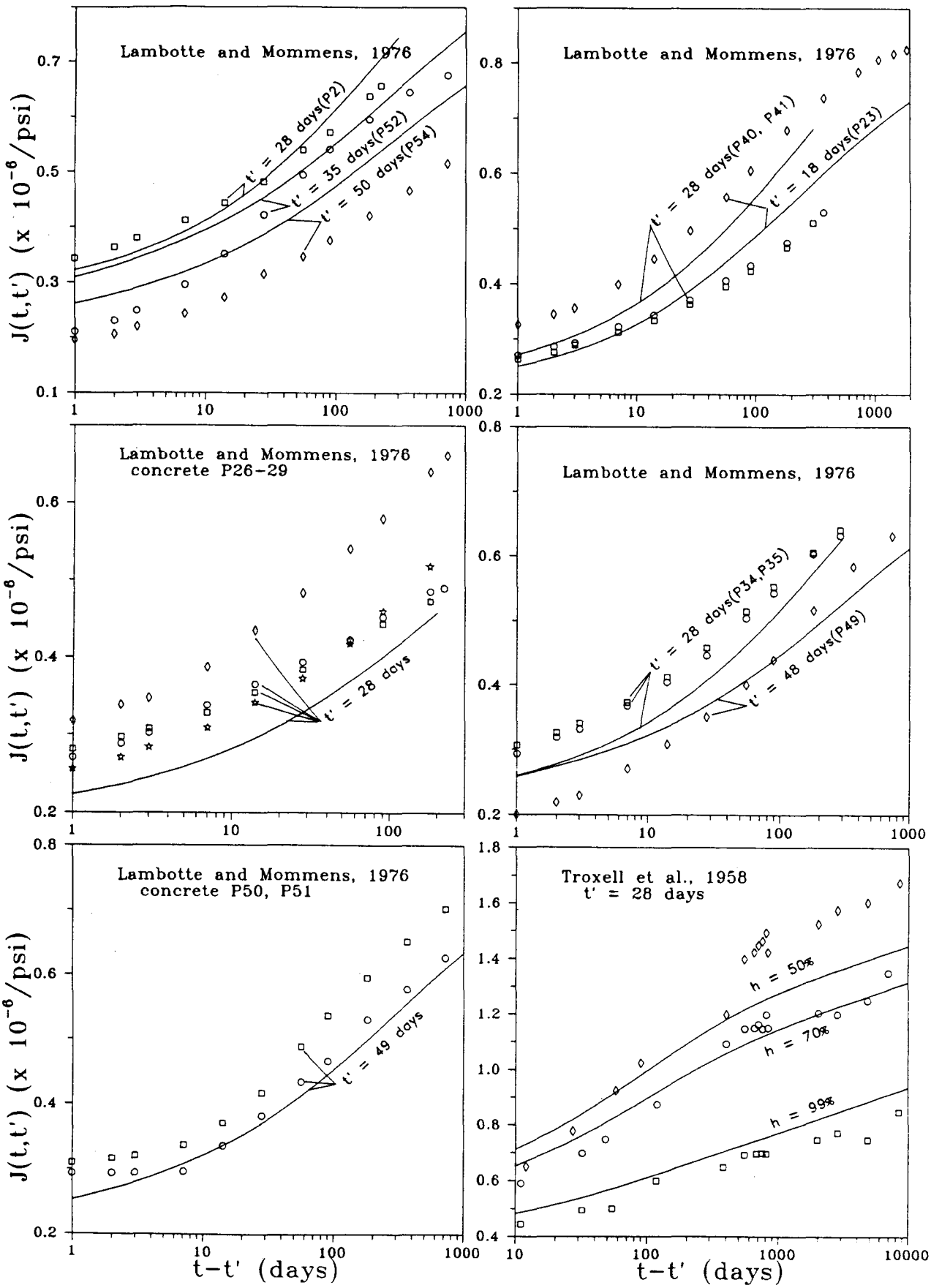

Fig. 2 Predictions of drying creep and data by Lambotte and Mommens [11] and Troxell *et al.* [18].

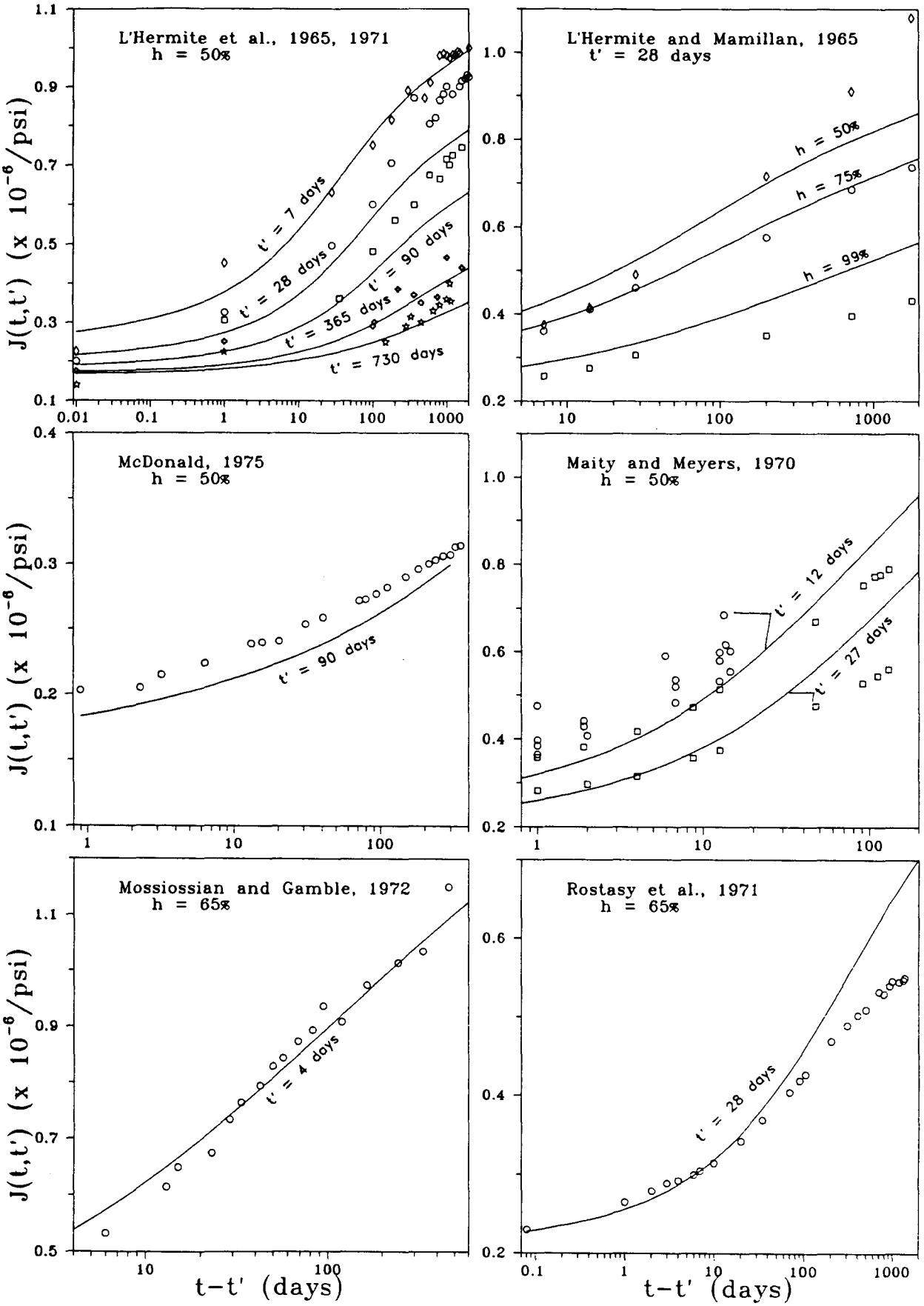

Fig. 3 Predictions of drying creep and data by L'Hermite *et al.* [12], L'Hermite and Mamillan [13], Maity and Meyers [14], McDonald [15], Mossiossian and Gamble [16] and Rostasy *et al.* [17].

5. COMPARISON WITH DRYING CREEP MEASUREMENTS

Using the same method as already described, the parameters of the present equations have been optimized so as to achieve least-square optimum fits of a set of 19 different comprehensive test data available in the literature [8–19]. The comparisons are exhibited in Figs 1–4. It must be kept in mind that these comparisons involve material parameter predictions from strength and composition. As already pointed out, these predictions are the main source error seen in the figures. If each data set were fitted individually, the fits would be much closer.

The test data of McDonald [15] and York *et al.* [19] differ from the others in that the specimens were resealed at the time of loading. In that case function C_d in Equation 2 was neglected because no drying creep occurs. Furthermore, when the specimen is resealed before loading, the value of t' in Equation 4 should be replaced by age t_r at resealing.

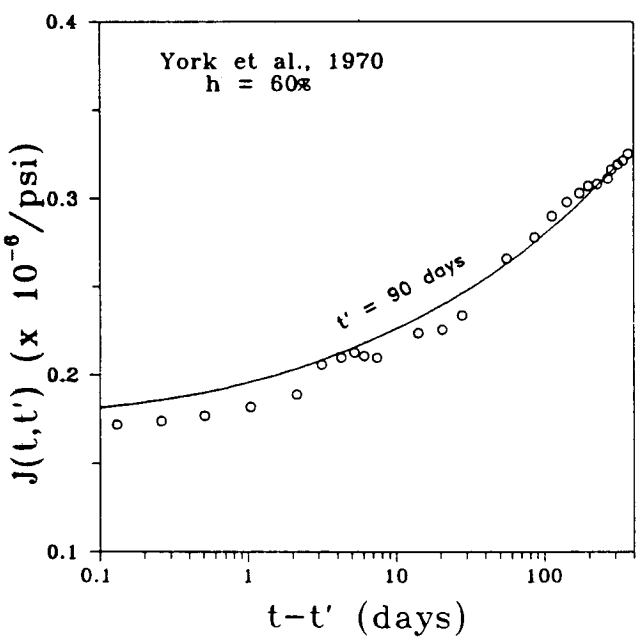

Fig. 4 Predictions of drying creep and data by York *et al.* [19].

The predictions shown in Figs 1–4 are generally better than those obtained with previous formulations. Especially, the data of L'Hermite *et al.* [12] for various ages of loading are predicted quite well. The comparisons with the data of Keeton [10] demonstrate good agreement for different environmental humidities. As for the data of Lambotte and Mommens [11], it should be noted that the curing conditions for these tests were quite unusual (the specimens were exposed to drying environment at the age of only 24 h).

The statistical scatter is characterized by the coefficients of variation (see Table 1), which were calculated in the same manner as in Parts 1 and 2 [4,5], described in detail in Part VI of Bažant and Panula [3].

Table 1 Coefficients of variation for deviations of formulae from the hand-smoothed data for drying creep

Test data	$\bar{\omega}$
Hansen and Mattock [8]	39.7
Hummel *et al.* [9]	20.7
Keeton [10]	8.2
Lambotte and Mommens [11]	16.8
L'Hermite *et al.* [12]	11.5
L'Hermite and Mamillan [13]	20.9
Maity and Meyers [14]	10.3
McDonald [15]	6.8
Mossiossian and Gamble [16]	2.9
Rostasy *et al.* [17]	15.9
Troxell *et al.* [18]	9.2
York *et al.* [19]	3.7
$\bar{\omega}_{all} = 16.9$	

6. EFFECT OF MICROCRACKING

The drying creep strain $\sigma C_d(t, t', t_0)$, also called the stress-induced shrinkage, includes the effects of microcracking (or cracking) and of pore humidity rate on the apparent creep viscosities, both of which are almost equally important [20,21]. In a specimen under sufficient compression the observed shrinkage is much closer to the true material shrinkage (free shrinkage of a small element) than in a load-free specimen. The reason is that the shrinkage observed on a load-free specimen is significantly offset by microcracking.

This is true also of the final values, because microcracking is largely irreversible (the cracks, once formed, cannot close completely). This phenomenon causes the average cross-section shrinkage to depend on stress, which is taken into account by the term $\sigma C_d(t, t', t_0)$.

The microcracking can be enhanced by restraint which reduces the shrinkage strain; the term $\sigma C_d(t, t', t_0)$ is essential for realistic calculation of shrinkage stress in restrained concrete beams or slabs.

APPENDIX: Basic information on drying creep data used

Hansen and Mattock [8]. Cylinders of diameters $d =$ 10.2 to 60 cm, and lengths 45.7, 55.9, 66.0, 86.4, 106.7, 127.0, 147.3 cm; 2 days in mould, 6 days in fog at 70°F (21°C). At the age of 8 days the specimens were loaded and exposed to 50% relative humidity. 28-day cylinder strength 6000 psi (41.4 N mm^{-2}). Elgin gravel (92% calcite, 8% quartz), maximum aggregate size 0.75 in. (19 mm). ASTM type III cement, content 303 kg m^{-3}; water:cement:sand:gravel ratio = 0.71:1:3.3:2.7. Axial compressive stress = 1200 psi (8.3 N mm^{-2}).

Hummel et al. [9]. After 7 days of curing, cylinders 20 cm × 80 cm were transferred to an environment of relative humidity 65% and temperature 20°C. Axial load applied at age of 28 days. Mix A: Portland cement PZ225, content 350 kg m^{-3}; water:cement:aggregate ratio = 0.38:1:5.4. 28-day cylinder strength 414 kg cm^{-2} (40.6

N mm^{-2}). Mix B: Cement Z425, content 334 kg m^{-3}; water: cement:aggregate ratio = 0.55:1:5.4. 28-day cylinder strength 435 kg cm^{-2} (42.7 N mm^{-2}). Specimens loaded at the ages of 3, 28 and 90 days. Rhine gravel, maximum size 30 mm.

Keeton [10]. At the age of 24 h the specimens were demoulded and placed in 100% relative humidity. Load was applied and specimens were exposed to drying at 75°F (24°C) at age of 8 days. Portland cement type III, content 451.2 kg m^{-3}; water:cement:sand:gravel ratio = 0.46:1:1.66:2.07; maximum aggregate size 0.75 in. (19 mm); fine aggregate, Saticoy River sand; coarse aggregate, Santa Clara River gravel. 28-day cylinder strength 6550 psi (45.2 N mm^{-2}).

Lambotte and Mommens [11]. High-strength Portland cement, except concretes P40 and P41, in which early-strength cement was used. Specimens cured in mould for 24 h, then exposed to drying environment of 20°C and relative humidity 60%, except 95% for concretes P49–P54. Specimens P2 to P41 were of size 15 cm × 15 cm × 60 cm, specimens P49 to P54 of size 10 cm × 10 cm × 40 cm. For further data see Table 2, in which t' is in days, f_c^* is cube strength at the time of loading (N mm^{-2}), c is cement content (kg m^{-3}) and $w{:}c{:}s{:}g$ is water:cement: sand:gravel ratio.

L'Hermite et al. [12]. Prisms 7 cm × 7 cm × 28 cm cured in water; at $t_0 = 2$ days exposed to drying at 50% relative humidity and 20°C. Portland cement, content 350 kg m^{-3}; water:cement:sand:gravel ratio = 0.49:1:1.75:3.07. 28-day strength 370 kg cm^{-2} (36.3 N mm^{-2}). Seine gravel (siliceous calcite), maximum aggregate size 20 mm. Axial compressive stress 1315 psi (9.07 N mm^{-2}).

L'Hermite and Mamillan [13]. Specimens 7 cm × 7 cm × 28 cm cured in water 28 days, loaded at the age of 28 days and exposed to drying at relative humidities 50, 75 and 99%, and temperature 20°C. Cement French type 400/800, content 350 kg m^{-3}; water:cement:sand:gravel ratio = 0.49:1:1.75:3.07. 28-day strength 370 kg cm^{-2} (36.3 N mm^{-2}). Seine gravel (siliceous calcite), maximum size of aggregate 20 mm. Axial compressive stress 1422 psi (9.80 N mm^{-2}).

Table 2 Additional data for Lambotte and Mommens' tests [11]

Concrete	t'	f_c^*	c	$w{:}c{:}s{:}g$
P2	28	32.6	270	0.611:1:2.33:4.74
P13	28	40.5	350	0.5:1:1.71:3.56
P26–P29	28	53.3[a]	400	0.351:1:1.06:3.49
P23	18	52.7	360	0.445:1:1.76:3.55
P31	7	47.6	400	0.575:1:1.71:3.04
P32	28	46.8	400	0.4:1:1.5:3.17
P34, P35	28	51.2	400	0.45:1:1.5:3.17
P40, P41	28	52.0	450	0.433:1:1.28:2.82
P49	48	49.8	350	0.48:1:1.85:3.71
P50, P51	49	56.6	350	0.49:1:1.85:3.59
P52	35	57.3	362	0.47:1:1.79:3.98
P54	50	45.2	350	0.52:1:1.85:3.71

[a]Average of four.

Maity and Meyers [14]. Prisms 14 in. × 3.5 in. × 3.5 in. (356 mm × 89 mm × 89 mm). After 4 days of curing exposed to 50% relative humidity and at 70°F (21°C) 12-day cylinder strength = 5200 psi (35.9 N mm^{-2}) on cylinder 4 in. × 8 in. Cement type III, content 253 kg cm^{-3}; water:cement:sand:coarse aggregate ratio = 0.85:1:3.81:3.81. Crushed limestone and quartz sand. Axial compressive stress 1740 psi (12.0 N mm^{-2}).

McDonald [15]. After 7 days of wet curing, cylinders 6 in. × 16 in. (152 mm × 406 mm) were allowed to dry for 75 days in air at 50% relative humidity and 73°F (23°C). Then the specimens were resealed. Load applied at the age of 90 days. 28-day cylinder strength = 6300 psi (43.4 N mm^{-2}). Portland cement type II, content 404 kg cm^{-3}; limestone, maximum size of aggregate 0.75 in. (19 mm); water:cement:sand:coarse aggregate ratio = 0.425:1: 2.03:2.62. Axial compressive stress 2400 psi (16.6 N mm^{-2}).

Mossiossian and Gamble [16]. Cylinders 6 in. × 12 in. (152 mm × 305 mm) were loaded and exposed to drying after 4 days of curing at 50% relative humidity and 70°F (21 C). Cement type III, content 418 kg m^{-3}; water: cement:sand:gravel ratio = 0.49:1:1.35:2.98. Coarse aggregate: crushed limestone, maximum size 1 in. (25.4 mm). 29-day cylinder strength = 7160 psi (49.4 N mm^{-2}).

Rostasy et al. [17]. Cylinders 20 cm × 140 cm exposed to drying after 7 days of curing at 65% relative humidity and 20°C. Axial load applied at the age of 28 days. 28-day cube strength 498 kg cm^{-2} (48.8 N mm^{-2}). Cement content 275 kg m^{-3}; water:cement:sand:gravel ratio = 0.56:1: 3.08:4. Rhine sand and Rhine gravel, maximum aggregate size 30 mm.

Troxell et al. [18]. Cylinders 4 in. × 14 in. (102 mm × 356 mm) exposed from the age of 28 days to relative humidities 50, 70 and 99%, and temperature 70°F (21°C). Water:cement:sand:coarse aggregate ratio = 0.59:1: 2:3.69. 28-day cube strength 2500 psi (17.2 N mm^{-2}). Cement type I, content 320 kg m^{-3}; granite aggregate, maximum size of aggregate 1.5 in. Axial compressive stress 800 psi (5.5 N mm^{-2}).

York et al. [19]. Cylinders 6 in. × 16 in. after 7 days of curing exposed to 60% relative humidity and 75°F (24°C). At age of 83 days the specimens were sealed in copper jackets. Load applied at age of 90 days. Portland cement type II, content 404 kg m^{-3}; limestone, maximum size of aggregate 0.5 in. Water:cement:sand:coarse aggregate ratio = 0.425:1:2.03:2.62. 28-day cylinder strength 6650 psi (45.9 N mm^{-2}).

REFERENCES

1. Bažant, Z. P., 'Material models for structural creep analysis', in 'Mathematical Modeling of Creep and Shrinkage of Concrete', edited by Z. P. Bažant (Wiley, Chichester and New York, 1988) pp. 99–215.
2. Bažant, Z. P. and Chern, J. C., 'Concrete creep at variable humidity: constitutive law and mechanism', *Mater. Struct.* **18**(103) (1985) 1–20.

3. Bažant, Z. P. and Panula, L., 'Practical prediction of time-dependent deformations of concrete', Parts I and II: *ibid.* **11**(65) (1978) 307–328, Parts III and IV: *ibid.* **11**(66) (1978) 415–434, Parts V and VI: *ibid.* **12**(69) (1979) 169–183.
4. Bažant, Z. P. and Kim, J.-K., 'Improved prediction model for time-dependent deformations of concrete: Part 2—Basic creep', *ibid.* **24** (1991) 409–421.
5. Bažant, Z. P., Kim, J.-K. and Panula, L., 'Improved prediction model for time-dependent deformations of concrete: Part 1—Shrinkage', *ibid.* **24** (1991) 327–345.
6. Simenov, I. and Bozhinov, G., 'Some features of the structure of cement stone influencing the creep mechanism of concrete', in *Proceedings of International Conference on Mechanical Behaviour of Materials*, Kyoto, Japan, 1972, Vol. IV, pp. 262–266.
7. Bažant, Z. P. and Wang, T. S., 'Practical prediction of cyclic humidity effect in creep and shrinkage of concrete', *Mater. Struct.* **18**(106) (1985) 247–252.
8. Hansen, T. C. and Mattock, A. H., 'Influence of size and shape of member on the shrinkage and creep of concrete', *ACI J.* **63** (1966) 267–290.
9. Hummel, A., Wesche, K. H. and Brand, W., 'Der Einfluss der Zementart, des Wasser-Zement-Verhältnisses und des Belastungsalters auf das Kriechen von Beton', Deutscher Ausschuss für Stahlbeton, Heft 146 (Ernst, Berlin, 1962) pp. 1–58.
10. Keeton, J. R., 'Study of creep in concrete', Technical Reports R333-I, R333-II, R333-III (US Naval Civil Engineering Laboratory, Port Hueneme, California, 1965).
11. Lambotte, H. and Mommens, A. L., 'L'évolution du retrait du béton en fonction de sa composition et de l'âge', Technical Report, groupe de travail GT22 (Centre national de recherches scientifiques et techniques et pour l'industrie cimentière, Bruxelles, 1976), and privately communicated unpublished data (1978).
12. L'Hermite, R. G., Mamillan, M. and Lefèvre, C., 'Nouveaux résultats de recherches sur la déformation et la rupture du béton', *Ann. Inst. Techn. Bâtiment Trav. Publics* **18**(207–208) (1965) 323–360; see also International Conference on the Structure of Concrete (Cement and Concrete Association, London, England, 1968) pp. 423–433.
13. L'Hermite, R. G. and Mamillan, M., 'Influence de la dimension des éprouvettes sur le retrait', *ibid.* **23**(270) (1970) 5–6.
14. Maity, K. and Meyers, B. L., 'The effect of loading history on the creep and creep recovery of sealed and unsealed plain concrete specimens', Report No. 70-7, NSF Grant GK-3066 (Department of Civil Engineering, University of Iowa, Iowa City, 1970).
15. McDonald, J. E., 'Time-dependent deformation of concrete under multiaxial stress conditions', Technical Report C-75-4 (Concrete Laboratory, US Army Engineering Waterways Experiment Station, Vicksburg, Miss., 1975).
16. Mossiossian, V. and Gamble, W. L., 'Time-dependent behavior of non-composite and composite prestressed concrete structures under field and laboratory conditions', Structural Research Series No. 385, Illinois Cooperative Highway Research Program, Series No. 129 (Civil Engineering Studies, University of Illinois, Urbana, 1972).
17. Rostasy, F. S., Teichen, K.-Th. and Engelke, H., 'Beitrag zur Klärung des Zusammenhanges von Kriechen und Relaxation bei Normal-beton', Amtliche Forschungs- und Materialprüfungsanstalt für das Bauwesen, Heft 139 (Otto-Graf-Institut, Universität Stuttgart, Strassenbau und Strassenverkehrstechnik, 1972).
18. Troxell, G. E., Raphael, J. E. and Davis, R. W., 'Long-time creep and shrinkage tests of plain and reinforced concrete', *Proc. ASTM* **58** (1958) 1101–1120.
19. York, G. P., Kennedy, T. W. and Perry, E. S., 'Experimental investigation of creep in concrete subjected to multiaxial compressive stresses and elevated temperatures', Research Report 2864-2 to Oak Ridge National Laboratory (Department of Civil Engineering, University of Texas, Austin, June 1970); see also 'Concrete for Nuclear Reactors', American Concrete Institute Special Publication No. 34 (1972) pp. 647–700.
20. Bažant, Z. P. and Chern, J. C., 'Strain-softening with creep and exponential algorithm', *J. Engng Mech. ASCE* **111** (EM5) (1985) 391–451.
21. *Idem*, 'Stress-induced thermal and shrinkage strains in concrete', *ibid.* **113**(10) (1987) 1493–1511.

RESUME

Modèle amélioré de prédiction des déformations du béton en fonction du temps: 3ème partie – Fluage au séchage

Dans le troisième volet de cette série, on présente les formules de prédiction pour la fonction de compliance moyenne dans la section transversale d'une éprouvette soumise au séchage à température constante. Les formules décrivent le fluage additionnel causé par le séchage au moyen de la fonction de retrait qui introduit automatiquement les aboutissements de la théorie de diffusion, tels ceux qui font dépendre le fluage de l'épaisseur et de la forme de la section transversale. On compare les formules de prédiction à 19 séries de données prises dans la littérature, qui présentent une assez bonne concordance, supérieure à celle obtenue avec les modèles précédents. La source principale d'erreur réside dans une connaissance insuffisante du dosage et de la résistance du béton. On conseille d'éviter cette erreur en effectuant des mesures à court terme chaque fois que c'est possible.